ResearchGate

See discussions, stats, and author profiles for this publication at: https://www.researchgate.net/publication/373022312

Numerical study on the effect of different column shapes on punching shear behavior of flat slabs

Article *in* Results in Engineering · August 2023

DOI: 10.1016/j.rineng.2023.101345

CITATION
1

READS
81

4 authors:



Mutiu Akinpelu
Kwara State University
30 PUBLICATIONS **206** CITATIONS
SEE PROFILE



D.s. Gabriel
Kwara State University
2 PUBLICATIONS **2** CITATIONS
SEE PROFILE



Ash-Shu'ara Marafa Salman
Kwara State University
14 PUBLICATIONS **26** CITATIONS
SEE PROFILE



Ibrahim Abiodun Raheem
University of Georgia
8 PUBLICATIONS **14** CITATIONS
SEE PROFILE

All content following this page was uploaded by Mutiu Akinpelu on 15 August 2023.

The user has requested enhancement of the downloaded file.

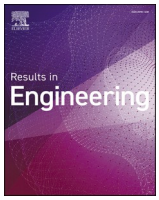
Results in Engineering 19 (2023) 101345



Contents lists available at ScienceDirect

Results in Engineering

journal homepage: www.sciencedirect.com/journal/results-in-engineering



Case report

Numerical study on the effect of different column shapes on punching shear behavior of flat slabs

M.A. Akinpelu [a,*], D.S. Gabriel [a], A.M. Salman [a], I.A. Raheem [b]

[a] Department of Civil Engineering, Faculty of Engineering and Technology, Kwara State University, Malete, Kwara State, Nigeria
[b] College of Engineering, Resilient Infrastructural Systems, University of Georgia, Athens, United States

ARTICLE INFO

Keywords:
Flat slabs
Punching shear
Concrete damage plasticity
Finite element model
Column shapes

ABSTRACT

This study was carried out to assess the punching shear behavior of flat slabs considering the use of various column shapes such as L, T, and Cruciform as support. The flat slab floor system is becoming most adopted in various structures ranging from medium-rise to skyscrapers, garages, factories, airports, etc. Although in this field of study, various research has been carried out over the decade, limited considerations were made for compound column geometries. Finite Element modelling software Abaqus was used in the development of a numerical model capable of predicting punching shear features of flat slabs. The control model was a flat slab supported on a square column established from an experimental test reported in previously published literature. The concrete material behaviour was defined in the Concrete Damage Plasticity Model and the best-suited parameters were deduced by sensitivity analysis. A comparative analysis was performed to compare the numerical results to both experimental and code predictions from ACI 318-19, Eurocode 2, 2004 and Model Code 2010. The study revealed that the shape of columns influences the punching shear capacity, with L, T, and Cruciform giving an increase of 3%, 5.2% and 22.6% respectively.

1. Introduction

Flat slabs are indisputably the most common forms of slabs after solid and rib systems of flooring in buildings. This system of flooring nullifies the intermediate load-transferring elements such as beams and enables direct transmission of loads that are exerted on the slabs to be transferred to the columns being its primary support [1]. These types of slabs are becoming more preferred due to their numerous advantages over other categories of slabs. These include higher headroom, reduced building height, faster rate of construction, and reduced cost of construction [2].

Typically, a flat slab is highly susceptible to a brittle structural failure known as Punching shear [3]. This structural phenomenon occurs because of highly concentrated stresses that exist around the regions of the supporting columns [4]. Punching shear is known to be an undesirable mode of failure in that it occurs without any preceding notice on the physical appearance of the slab. This, as result, can lead to the progressive collapse of large areas of slab or even complete structures. Although, most punching failure occurs at the earliest stage during construction when concrete is yet to harness its optimal strength to resist the shear effects [5]. Nevertheless, previous occurrences have shown that even in the post-construction phenomenon, buildings in service are not exempted from this failure so as much during construction [6].

Beyond seeming like a simple phenomenon, punching shear failure is complex and highly variant. This is evident by various codes and professionals not finding a consensus method and values to predict its internal, external, pre-punching, and post-punching behavior. Attributing factors to these anomalous characteristics in strength and functionality include; size, orientation, and geometry of the column and slab, ratio and arrangement of reinforcement (with or without shear reinforcement), flexural characteristics of the slab, the constituent materials and their properties, etc. [7]. The parameters of supporting columns cannot be underestimated in flat slab structures. In fact, one among other attributes of the punching shear failure of the Sampoong department store in Seoul as noted by Park, (2011) was that the design specifications of columns were discovered to be compromised during the construction of the building, both in dimensions and arrangement [6]. Therefore, the impact of geometry and orientation of columns supporting flat slabs on punching shear resistance is worthy of research.

Extensive research has been conducted and reported in literature on

* Corresponding author.
E-mail address: mutiu.akinpelu@kwasu.edu.ng (M.A. Akinpelu).

https://doi.org/10.1016/j.rineng.2023.101345
Received 31 May 2023; Received in revised form 1 August 2023; Accepted 3 August 2023
Available online 9 August 2023
2590-1230/© 2023 The Author(s). Published by Elsevier B.V. This is an open access article under the CC BY-NC-ND license (http://creativecommons.org/licenses/by-nc-nd/4.0/).

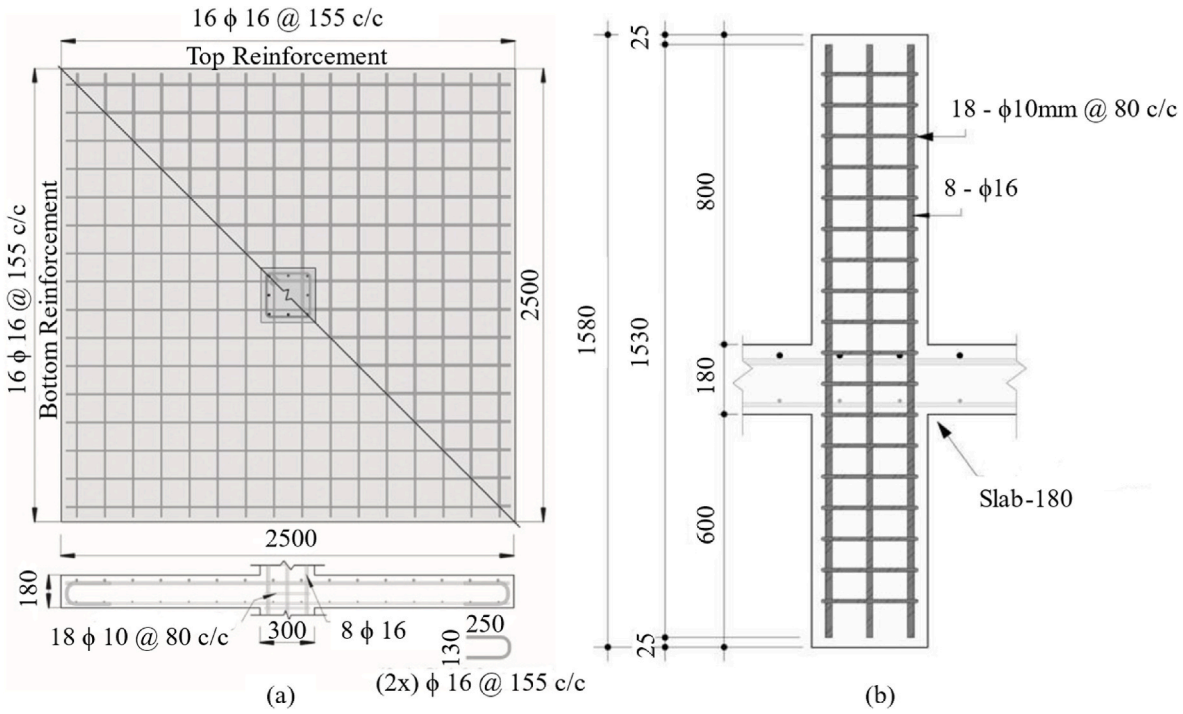


Fig. 1. (a) Slab reinforcement details (b) Column reinforcement details used in the experimental test (all dimensions in mm) [26,28].

reinforced concrete flat slabs.

[8–13]. Notwithstanding, due to the cost and time required to conduct experimental tests, the existing databases are still not sufficient to address structural issues relating to the punching shear behavior of flat slabs [14,15]. With the growing emergence of architectural designs, new, complex, irregular, and unconventional column shapes are becoming common in building designs [16]. Although, most of the design codes made provisions to be used for design against punching shear in flat slabs supported by non-square columns such as rectangular, L, T, and circular shapes, the empirical tests used in the development of the supposedly made provisions have given none to only a few considerations for other irregular shapes. Even the popular rectangular shape was said to have been given limited attention [17]. Therefore, the evaluation of strength properties of flat supported on irregular shapes cannot be over-emphasized.

Ever since the introduction of numerical methods in civil engineering, finite element models have been successfully applied to solve both simple linear and complex nonlinear problems [18]. Of all the finite element-based models available in the literature, the concrete damage plasticity model is mostly adopted for the simulation of reinforced concrete structural phenomena due to its unique capability to capture the entire behavior of reinforced concrete material including elastic, plastic, failure, and post-failure responses [19–21]. Wasatko et al. [22] applied the damage plasticity model as incorporated in Abaqus finite element software to predict the punching shear of a previously tested reinforced concrete flat slab-column connection. Genikomsou and Polak [23] also utilized concrete damage plasticity model in Abaqus software package to investigate failure modes of reinforced concrete slab-column connections subjected to static and pseudo-dynamic loadings and reported that the developed model accurately predicted the punching shear behavior of the studied slab specimens. The influence of load-induced thermal strain on the punching shear behavior of flat slabs at elevated temperatures was also studied by Al Hamd et al. [24] using Abaqus finite element software. In another study, Al Hamid et al. [25] also employed Abaqus software to study the effectiveness of the newly introduced shear head reinforcement on the punching shear capacity of slab-column connection subjected to eccentric load and fire. Milligan et al. [17]; Zhang et al. [14] researched flat slabs supported on rectangular and L-shaped columns respectively using nonlinear finite analysis, they concluded that the geometry of the supports is of significant influence on the punching shear behavior of flat slabs and proposed further that works should be conducted to consolidate the provisions of the code. The outcomes of all the studies revealed the unique capability of the software package in the simulation of the punching behavior of flat slabs.

In the present study, Abaqus finite element software was used to model and analyze the punching shear behavior of reinforced concrete slabs supported on columns of different geometrical shapes. Numerical model of a flat slab supported on a square column was developed according to the experimental results obtained from the literature, and then, the models were further extended to investigate the effects of column shapes on the punching shear behavior of flat slabs. Finally, the finite element results were compared to the provisions made by Eurocode, ACI and Model code. The outcomes of this study would guide structural engineers, architects, and designers in selecting the best-suited column geometries during design. Also, it would make an additional numerical database for researchers, particularly in terms of irregular column shapes considered in the course of this research namely; L, T, and Cruciform shapes.

2. Research methodology

The research was conducted in two stages. The first phase involves finite element modelling of a previously experimented reinforced concrete flat slab supported on a square column using the Abaqus modelling tool. The model output was therefore validated with the results of the selected experimental study as recorded in the literature. In the second stage, parametric analysis using column shape as a variable was carried out to determine the impact of column geometry on the characteristic load-deflection response, crack pattern, and failure loads of the slab.

2.1. Description of experimental test

To develop a 3D nonlinear finite element model of a flat slab and

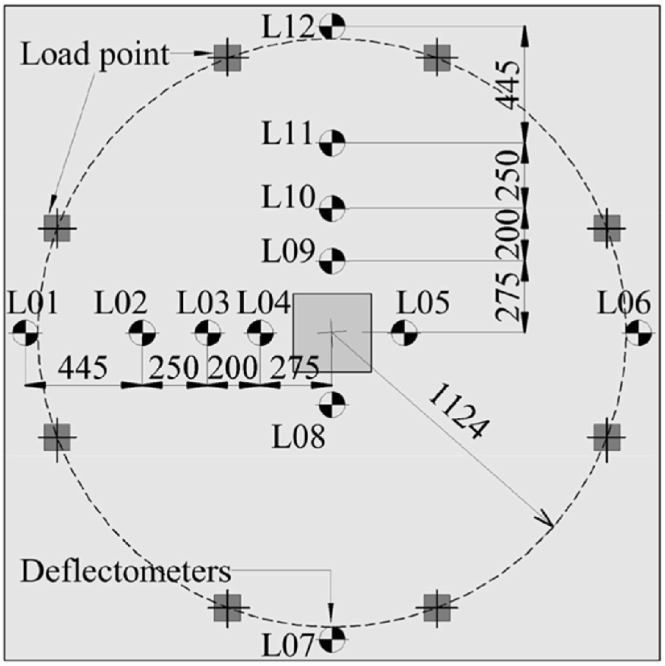


Fig. 2. Loading and deflectometer arrangements in experimental test (all dimensions mm) [26,28].

confirm its accuracy to an experimental set-up imitated, A flat slab specimen tagged RS, out of a series of test specimens experimented for punching at the University of Brasilia and reported by Refs. [26,27] was adopted. The test consists of a square flat slab of 2.5 m × 2.5 m supported by an internal column of 300mm × 300mm. The depth of the slab was 180mm reinforced with 16mm φ @155mm c/c (percentage of reinforcement ρ = 0.9) mm both ways at the tensile zone and 10mm φ @155mm c/c at the compressive zone. To fully ascertain the practical existence of such a structure, the column was monolithically connected with the slab protruding through the top and bottom of the slab by 800mm and 600mm respectively. The column was reinforced with 8nos of 16mm φ with links of 10mm φ at 80mm c/c. Further details are shown in Fig. 1a-b.

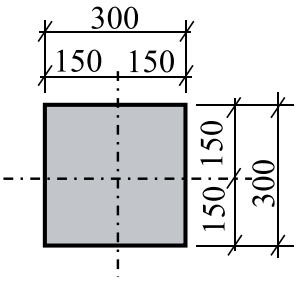
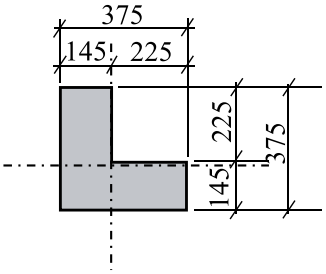
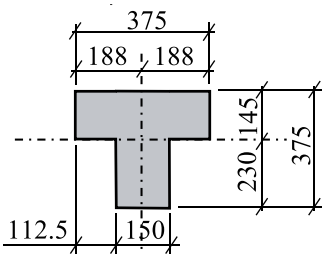
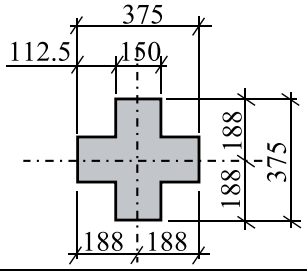
The research aimed to examine the influence of the variation of anchoring of shear reinforcement in flat slabs. The control slab RS without any shear reinforcements was constructed in the laboratory and tested against other samples of the flat slab which has stirrups serving as shear reinforcement. The slabs were loaded to failure by gradual increment through hydraulic jacks at 8 distinct points having radial dimensions of 1124 mm from the centre of the column as shown in Fig. 2.

2.2. Modelling with other column shapes

The major aim of developing numerical modelling is to enable a basis for performing a parametric variation that could not be fully covered by experiments. After validation and calibration of the numeric model with the experimental results, the calibrated model was used to study the effects of various column shapes. Three other models were developed, each model was characterised by the column shape which supports the flat slab. The column shapes considered are L, T, and Cruciform and each model was named after the shapes respectively.

Since none of the central axes of the L-shape model was symmetric with the column, a full model was developed. In the case of the T-shape column model, the model adopted was half (½) of the real model since one axis of symmetric exists that propagated similar response on both sides. To cater for the other half region, a factor of 2 was applied to multiply loading results during the simulation. The cruciform shape

Table 1
Parameters of columns used in modelled flat slabs.

Flat slab code	Column dimensions (mm)	Column area (mm^2)	Column perimeter (mm)
Square		90, 000	1200
L-shape		90, 000	1500
T-shape		90, 000	1500
Cruciform		90, 000	1500

coulmn has two (2) lines of symmetry along both X and Y axis which infers that the behaviour of one region is replicated in the other regions. Therefore, to reduce the computational cost, one-fourth (¼) of the model was adopted for the analysis and a factor of four (4) was applied in the determination of loads to cater for the unmodelled regions. In all the models it was ensured that the actual load area remains the same as well as the column perimeter as given in Table 1. This approach has been successfully adopted by various researcher when conducting numerical researchers [29–31].

The centroid of the column geometries was determined and positioned to coincide with that of the flat slab to ensure Zero (0) eccentricity in the model. Fig. 3a-d shows the plans as adopted in the modelling of various shapes with indications of the critical perimeter as specified in different building codes considered.

3. Finite element study

The multipurpose FE software, Abaqus (Dassault Systèmes, 2021) was used to develop the FE model and simulate the punching shear behaviour of the stated specimen of the flat slab. Abaqus software visualization module was used to provide a detailed output of stress and

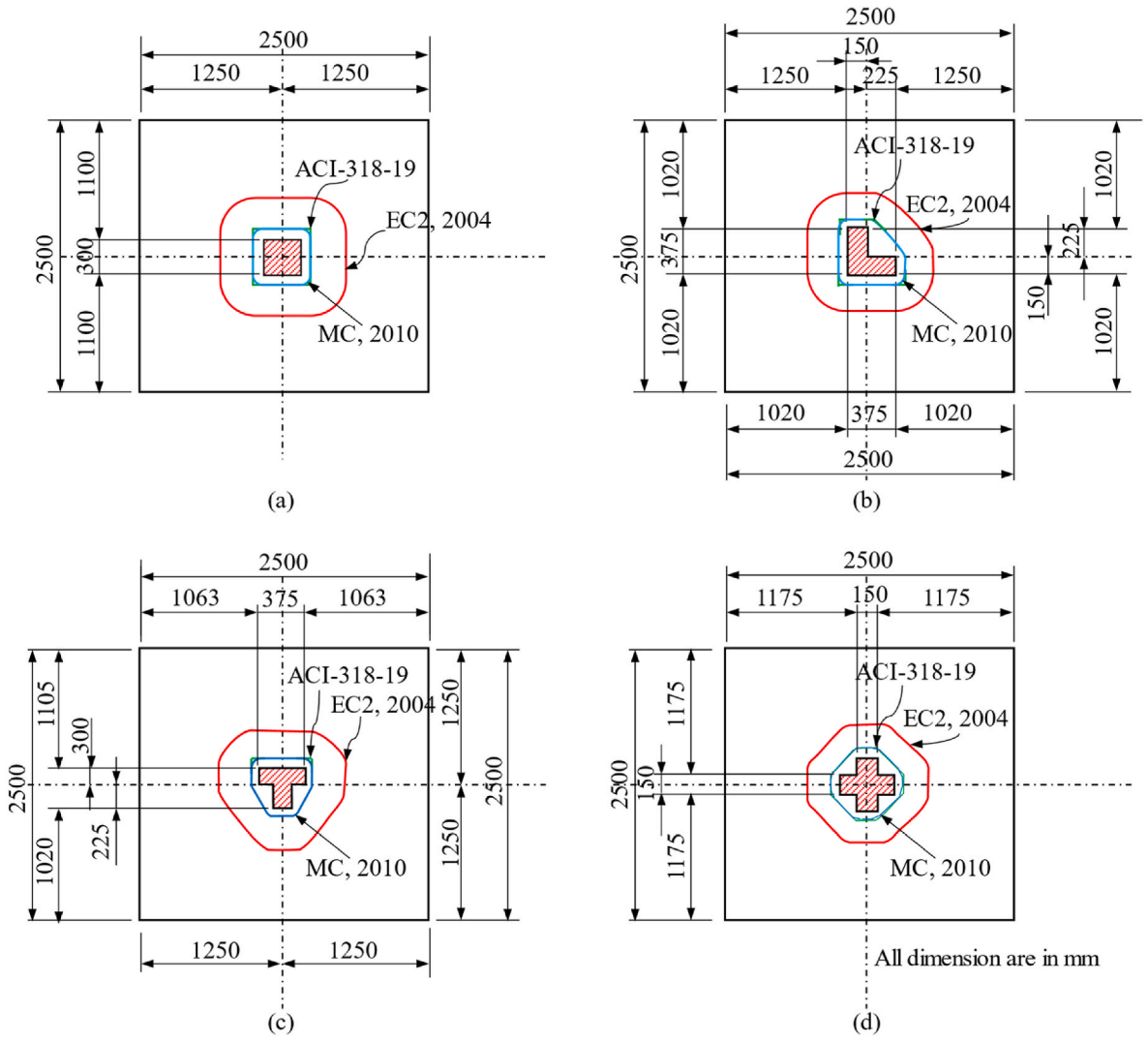


Fig. 3. Layouts of modelled flat slabs showing critical punching perimeter as per various code provisions: (a) Square column (b) L-shape (c) T-shape (d) Cruciform shape.

strain fields exhibited by the materials and the experimental circumstances simulated. The flat slab model was calibrated per the experimental results of the test, and then, the model was modified to study the impacts of column shapes on the punching shear behavior of flat slabs.

3.1. Materials Constitutive model

3.1.1. Concrete material behaviour

Concrete as a composite material with distinctive behaviour and properties was inherently developed as a unique module in the Abaqus software library. As stated by Dassault Systèmes [32], concrete material-inelastic behaviour can be calibrated into the Abaqus software using 3 approaches namely: Concrete Smear Cracking, Cracking model for concrete, and Concrete damage plasticity model. However, previous studies [28,33,34] have reported that CPDM is the most preferred and generally the agreed model for imitating the virtual characteristics of concrete components under various actions of load and stresses. The use of CPDM has been validated by many researchers and it was found to have the most precise results compared to experimental values and observations during loading, at failure, and post-failure of reinforced concrete structures [35–38]. According to Dassault Systèmes [32], the yielding criterion was based on the theory postulated by Lubliner et al. (1989) [39] incorporated with modifications proposed by Lee et al. (1998) [40]. The mechanical properties of the materials as reported in the experimental study (Table 2) were adopted in the definition of CDPM parameters.

Table 2
Mechanical properties for the concrete [27].

Slab	mean compressive strength, fc (N/mm2)	Average tensile strength, ftm (N/mm2)	Modulus of Elasticity (N/mm2)
RS	29.9	2.89[a]	32,810[b]

The average tensile strength and elastic modulus of concrete were calculated using Eurocode 2 (2004) as stated in Eqns (1) and (2) respectively.

a) $f_{tm} = 0.3 * f_c^{2/3}$ (1)

b) $E_C = 22\ [\ (f_c + 8)/10]^{0.3} * 10^3$ (2)

3.1.1.1. Definition of CDPM parameters. The degree of accuracy of the numerical model and its simulating coherence with the test observed results is largely dependent on the parameters defined by the user in the CPDM module. The calibration of CPDM involves 3 different phases which include the Plasticity, Compressive behaviour and Tensile

behaviour stage of the concrete. The theories and governing equations considered are discussed in the subsequent sections.

3.1.1.2. Concrete in compression. Only the ultimate compressive strength of the concrete after 28 days was indicated in the adopted literature. Therefore, analytical theories and equations are the most suited alternatives to provide such data, as it is an essential input required for the precise calibration of the model.

The compressive stress and shortening strain for short-term uniaxial loading relationship was adopted from Equations (3)–(9) as defined in Eurocode 2, 2004 [41].

$$\frac{\sigma_c}{f_{cm}} = \frac{k\eta - \eta^2}{1 + (k-2)\eta} \tag{3}$$

The denotations in Eqn (3) are as defined in Eqns. (4)-(9)

$$\eta = \frac{\varepsilon_c}{\varepsilon_{c1}} \tag{4}$$

$$\varepsilon_u = 0.0035 \ \left(f_c < 50 \text{ N} / \text{mm}^2\right) \tag{5}$$

$$\varepsilon_{c1} = \left(\frac{0.7 f_{cm}^{0.31}}{100}\right) < 2.8 \tag{6}$$

$$\varepsilon_{cu} = \left(2.8 + 27\left[(98 - f_c)/100\right]^4\right) \ \left(f_c < 50\ N/mm^2\right) \tag{7}$$

$$k = 1.1 E_C \times \left(\frac{\varepsilon_u}{f_{cm}}\right) \tag{8}$$

$$f_{cm} = f_c + 8 \tag{9}$$

where:

f_c is the characteristic cylindrical compressive strength of concrete at 28 days.

f_{cm} is the mean value of concrete cylinder compressive strength.

ε_c is the strain at peak stress.

ε_{c1} is the ultimate strain.

As considered generally favorable for numerical implementations by Akinpelu et al. [18] the post-elastic region of the concrete compressive behaviour was defined using the inelastic (crushing) strain in place of crack opening. Consequentially, the compressive inelastic strain was deduced as the ultimate (total) strain less the elastic strain corresponding to undamaged material.

3.1.1.3. Tensile behaviour of concrete. The brittle nonlinear nature of concrete when subjected to tensile stress is preferably defined using the stress-crack displacement as against the stress-strain response used in predicting its compressive behaviour. This method reduces the influence of mesh sensitivity issues that may arise due to the unreinforced sections of the model on the corresponding numerical results. The stress-crack displacement relationship response can be expressed using either linear, bilinear, or exponential tension softening. The exponential tension softening curve is taken as postulated by Cornelissen et al., [42] and adopted by Genikomsou et al. [43] and was applied during this study.

The following analytical models are as defined suitable by Cornelissen et al. [42], with terms and symbols modifications from Genikomsou et al. [43].

$$\frac{\sigma}{f_t} = \left(\left(1 + \left(\frac{c_1}{w_c}\right)^3\right) e^{-\left(\frac{c_2 w}{w_c}\right)}\right) - \left(\left(\frac{w}{w_c}\right)\left(1 + c_1^3\right) e^{-c_2}\right) \tag{10}$$

$$w_c = 5.14\left(\frac{G_f}{f_t}\right) \tag{11}$$

where; c_1 and c_2 are materials coefficients determined to be 3 and 6.93 respectively and w_c is the critical crack opening width, f_t is the tensile strength of concrete. While G_F is as established in Ref. [44] denoting the energy needed to propagate a tensile crack of a unit area given in Eqn. (12);

$$G_F = G_{F0}\left(f_{cm}/f_{cmo}\right)^{0.7} \tag{12}$$

f_{cmo} is taken as 10, and G_{F0} is expressed as a coefficient which is dependent on the maximum aggregate size. Hence the derived value of 0.065 J/mm^2 is adopted as G_f assuming a maximum aggregate size d_{max} of 16mm.

3.1.1.4. Damage phenomenon in compression and tension. To fully capture the elastic degradation exhibited at the softening phase of the uniaxial stress-strain curve. Two independent variables d_t and d_c each having values ranging from 0 to 1 signifying the initially undamaged and total damage phenomena of the material were used respectively. The expressions in Eqn. (13) and Eqn. (14) were used to establish the resulting values of the damage variables.

$$d_c = 1 - \sigma_c/\sigma_{cmax} \tag{13}$$

$$d_t = 1 - \sigma_t/\sigma_{tmax} \tag{14}$$

where σ_c, σ_t are compressive and tensile stress respectively and σ_{cmax}, σ_{tmax} denotes maximum compressive and tensile stress respectively.

3.1.1.5. Other concrete damage plasticity model parameters.

(i) Dilation angle, ψ

Dilatancy is the resulting action of shear on the microstructural properties of concrete and soils leading to a positive increase in its initial volume [45]. A variety of dilation angles had been suggested by different researchers, therefore, making it a parameter without a unanimous value. Akinpelu et al. [46] validated a dilation of 56°. Szczecina et al. [47] recommended a value as low as 5°. Conversely, Genikomsou et al. [48] discovered a value of 40° gives a better correlation to the experimental observations. This was further corroborated by Beaulieu et al. [49] who as well noted that values between 35° to 40° were suitable. Here in, values dilation angles of 20°, 25°, 30°, 35°, and 40° were considered and the most correlating values were adopted for subsequent analysis.

(ii) Viscosity parameter, μ

This is similarly an essential parameter in CDPM calibration. Material models such as CDPM exhibiting softening behaviour and stiffness degradation mostly have a high unlikeliness to converge. Not only is there no definite value specified by the Abaqus software also there is no unified value agreed upon by researchers. To this end, a variety of literature did consider numerous values which are between 0.001-0.00001 [47,48]. Genikomsou et al. adopted a value of 0.00001. Szczecina et al. [47] concluded a value of 0.0001 was the most appropriate. Considering this, values of μ were varied as 0.001, 0.0001, and 0.0001 in other to determine the most applicable value.

iii) Flow Potential Eccentricity, ε

Changes are prevalent in the shape of tensile and compressive central axis under stress. As a result, eccentricity is associated with the shape of the surface and most importantly the edge nodes [45]. This default value of 0.1 has been generally undisputed across various research studies. By implication, ε is taken as the default value of 0.1 during this study.

iv) Stress Ratio, $\frac{\sigma_{bo}}{\sigma_{co}}$.

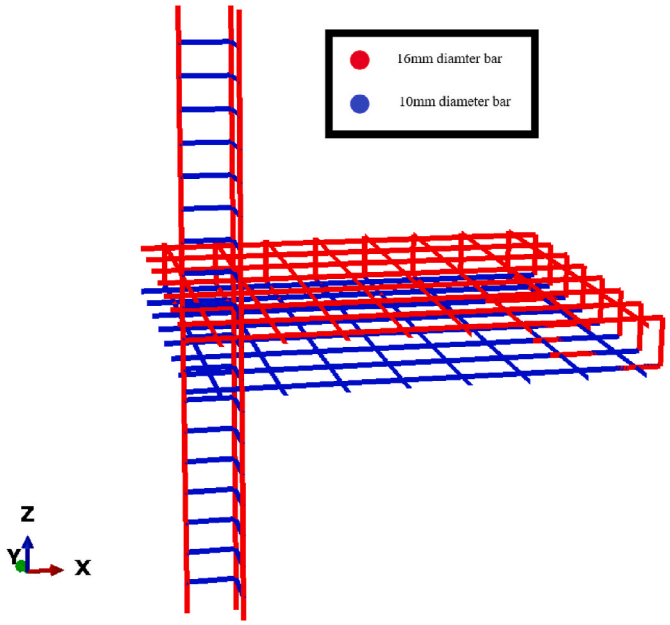


Fig. 4. Finite Element reinforcement model RS flat slab specimen.

Table 3
Mechanical properties for the reinforcement steel [27].

Bar diameter (mm)	Ultimate Yield stress (f_y) (N/mm^2)	Modulus of Elasticity (E_s) (N/mm^2)
16	549	196900
10	515	126600

The ratio of initial equibiaxial compressive yield stress to initial uniaxial compressive yield stress. This is a parameter that impacts the failure criterion of the material. It decides the point at which the material fails under biaxial compression. The default value of 1.16 is specified by Dassault Systèmes [32]. And herein adopted since it has been found as the most unified value used in previous numerical simulations by various authors.

v) K Parameter

This is the ratio of the second stress invariant on the tensile meridian to that on the compressive meridian at the initial yield for any given value of the pressure invariant such that the maximum principal stress is negative. It is within the limit of $0.5 < K \leq 1$ [50]. Genikomsou (2015) carried out a sensitivity analysis using values 0.667, 0.9, and 1 the findings showed that although this value has an impact on the results of the simulated model, its impact is largely negligible [48]. This observation influenced the choice of using a default value of 0.667 for all simulations.

3.1.2. *Steel reinforcement constitutive model*

Steel reinforcement material constituents behave similarly in both compression and tension, the widely adopted linear elastic, linear strain hardening model was used to define the stress-strain behaviour of the two types of steel reinforcement used in the model (i.e 16mm and 10mm as shown in Fig. 4). The reinforcement yield strength observed in the experiment (see Table 3) with zero (0) plastic strain was used to define the plasticity property of the material. In the adopted experiment, elastic modulus was 196,900 N/mm^2 and 126,600 N/mm^2 for 16mm and 10mm respectively. The results as observed in the experiment were adopted in the definition of steel bar behaviour and also the Poisson's ratio of 0.3 was used for the both diameter of bars.

3.1.3. *Finite element model aspects*

The concrete parts of the models were assigned a Concrete Three-Dimensional 8-node linear solid element (C3D8R). All reinforcements (as in Fig. 4) were modelled as Three Dimensional Two-node (T3D2) elements. The meshing density applied to the concrete parts of the model was 30mm (see Fig. 5a). The reinforcement meshing size was 15mm which indicates half of the element mesh of the concrete. It is noteworthy that the choice of mesh density stated was chosen based on the results of numerical research on the same experimental model carried out by Palhares et al. (2022).

The interaction and bond between the concrete and the steel reinforcement were defined using the embedded region available in the Abaqus constraint library. The loading process was applied using displacement control, the flat slab was loaded to failure by the imposition of downward displacement from the reference point which was located at a height away from the centre of the loaded surface (as used in the experimental set-up) and its interaction with the surface was defined using the Equation constraint in the Abaqus (Fig. 5b).

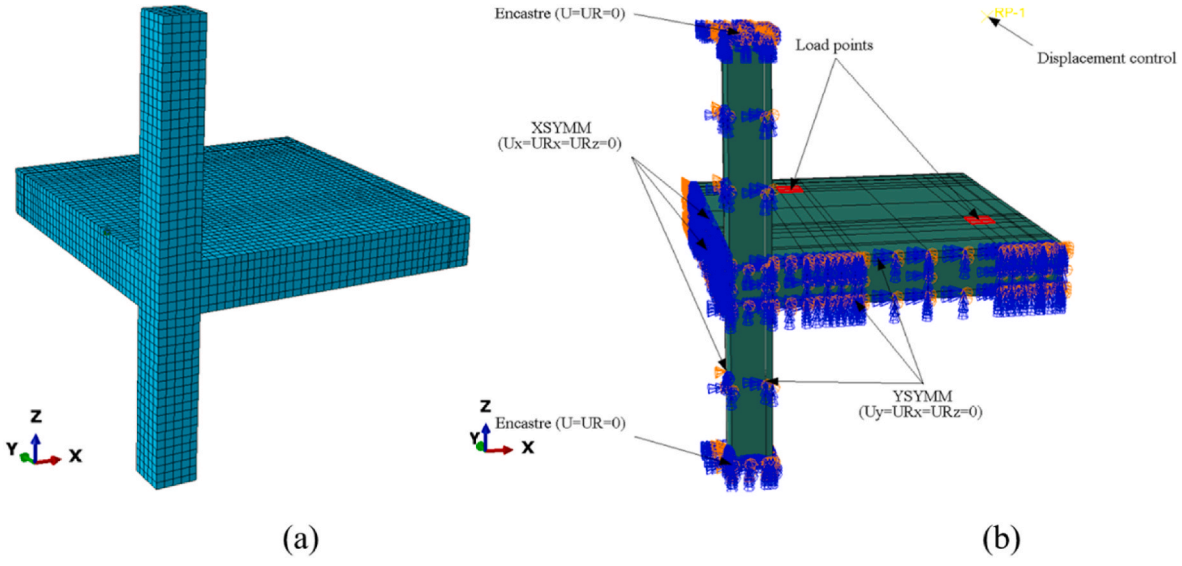


Fig. 5. FE model of RS specimen (a) Meshing (b) Boundary conditions and Loading points.

Table 4
Concrete Damage Plasticity parameter used during sensitivity analysis.

Dilation angle	Eccentricity	Stress ratio	K	Viscosity parameter
25	0.1	1.16	0.667	0.0001

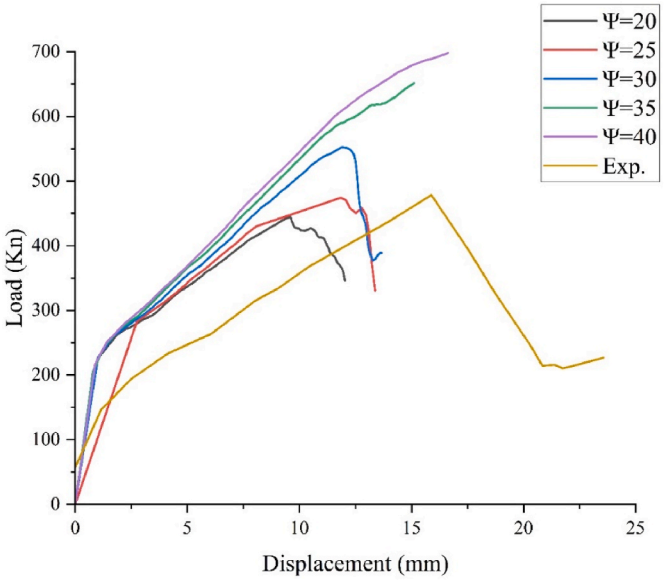


Fig. 6. Calibration of the dilation angle parameter.

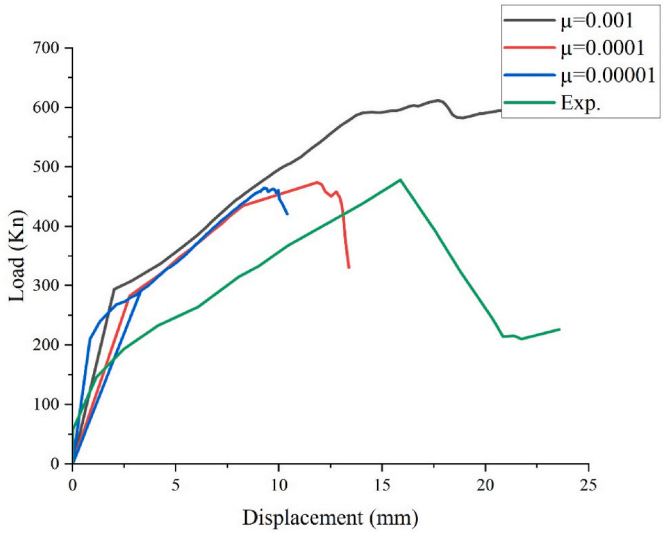


Fig. 7. Calibration of the viscosity parameter.

4. Results and discussion

4.1. Model calibration and validation

4.1.1. Model calibration

The values shown in Table 4 are the default while the dilation angle and viscosity parameters were varied to determine the appropriate value of use. The adoption of a best-suited dilation angle was further used during the variations of the other parameter.

4.1.1.1. Dilation angle parameter. Fig. 6 shows that dilation angles that give similar load-displacement behaviour comparatively to the experimental results are dilation angles 20°,25°, and 30°. Dilation angles of 35° and 40° give stiffer models which do not represent the true nature of punching failure as seen in the experimental response. Although values between 20° and 30° appear to show consistency with the punching resistance capacity and deformation pattern recorded during the physical test, there is a significant disparity in the deflection. The value of best conformity with the result of the test is 25° giving the most proximate relationship in terms of failure load and displacement.

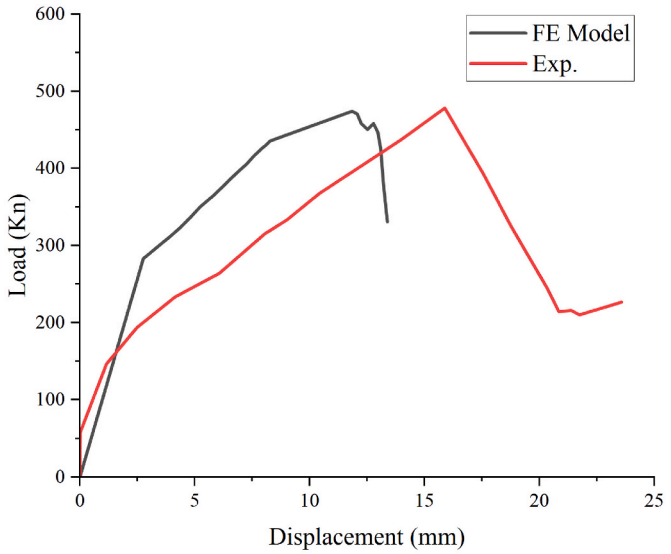


Fig. 8. Finite element versus experimental load-deflection response for the flat slabs.

4.1.1.2. Viscosity parameter. In contrast to the behaviour observed in the dilation angle, the trend observed in Fig. 7 shows that even higher viscosity parameters showed a true representation of the practical failure mode of punching. Notwithstanding, as viscosity increases, the precision of the model reduces. However, the use an extremely low viscosity parameter in the model could result in convergence difficulties and subsequently prompt an abrupt end to the analysis. Even though the most in-line value with the experimented model is 0.0001, 0.00001 also exhibits reasonable results compared to the experimental result but it is less ideal due to the analysis showing failure at an earlier stage of its non-linearity in contrast to 0.0001. The viscosity parameter used in the geometric variation and further analysis was therefore 0.0001.

4.1.2. Model validation

4.1.2.1. Load- displacement response. In the load-displacement graph of a flat slab, deflection increases as the load on the slab increases in the pre-punching phases of the slab. At the failure, a sudden drop in the load is usually experienced signifying the punching-resisting capacity of the slab. In the post-punching phase of the slab, further application of lesser loads implies larger deformation on the slab. This was the case of the finite element nonlinear graph as well as that recorded during the test which is shown in Fig. 8. It was observed that the finite element model indicates a stiffer response in the early stages of load application, such disparity has been discussed by Akinpelu et al. [43,46] who stated that

Table 5
Experimental versus Finite element.

Experimental		Finite element/Numerical		Relative Error (%)	
$V_{u,\,Exp}$	$\delta_{u,\,Exp}$	$V_{u,\,FEM}$	$\delta_{u,\,FEM}$	$\frac{V_{u.FEM}-V_{u.Exp}}{V_{u.Exp}}$	$\frac{\delta_{u.FEM}-\delta_{u.Exp}}{\delta_{u.Exp}}$
478.8	15.97	475.3	11.92	−0.73	25.36

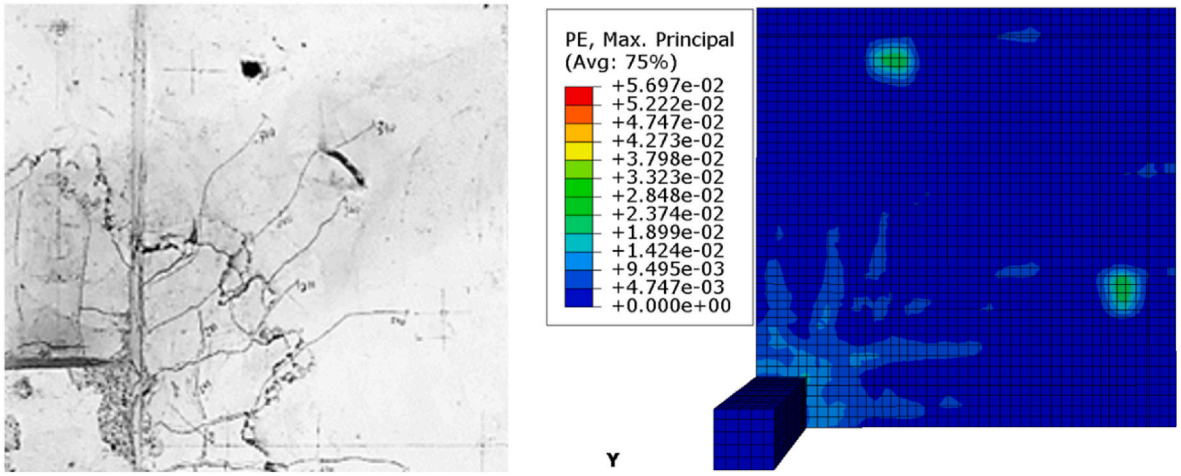


Fig. 9. Experiment crack map and finite element crack pattern at failure.

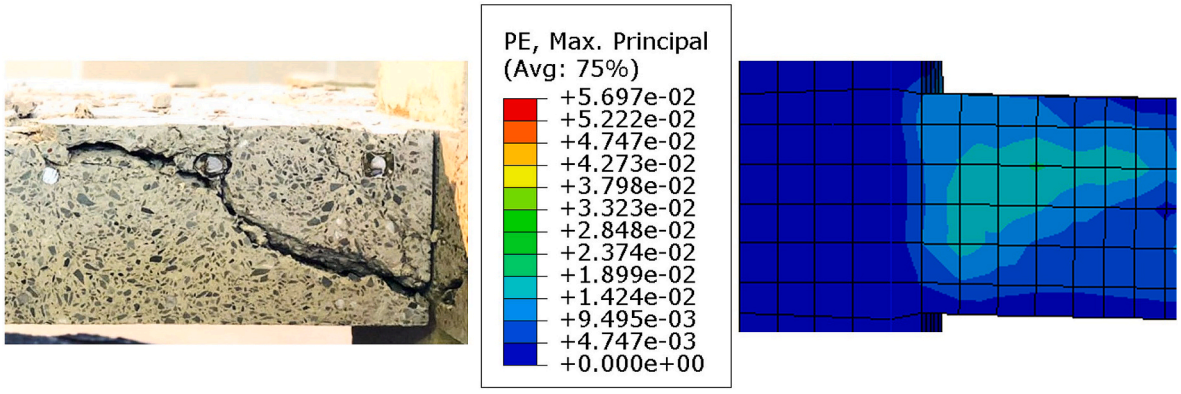


Fig. 10. Experimental versus FEM rupture surface at failure.

the development of micro-cracks which exist in the experimental model but cannot be detected by the experimental instrumentations could be a contributing factor to such occurrence. Regardless, the finite element model shows good coherence in the aspect of failure load and displacement when compared to the experimental inferences (see Table 5).

4.1.2.2. Crack pattern. The radial crack patterns propagating from the edges of the columns as recorded in the simulated slab model at peak load is in indicated in Fig. 9. Similar pattern was observed at the initial loading stage before failure. The punching cracks formed an undulated opening in an elliptical geometry around the column perimeter. The crack pattern marked in the experimental outcomes was in good correlation with that observed in the numerical analysis as shown in Fig. 9. Given the symmetric nature of the slab, the finite element model was one-fourth of the real model. Nonetheless, the numerical results show approximately symmetrical cracking properties with the test. It is important to highlight that within the concrete damaged plasticity model, the concept of cracks developing at the material integration point is not considered. However, the concept of an effective crack direction can be adopted for the purpose of visualizing the cracking patterns in the concrete structure. This premise assumes that cracking initiates at points where the tensile equivalent plastic strain is greater than zero and the maximum principal plastic strain is positive. Hence, the direction of the vector perpendicular to the crack plane is assumed to align with the direction of the maximum principal plastic strain, which can be visualized in the post-processor module of Abaqus CAE.

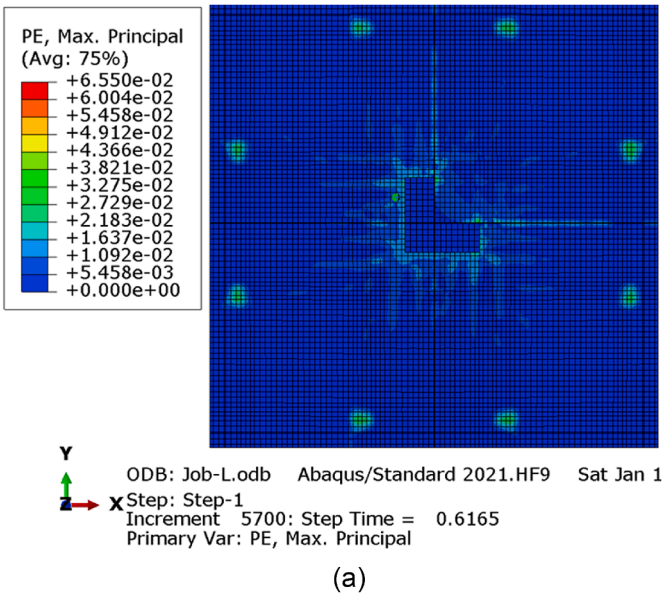


Fig. 11a. Crack pattern of L-Shaped column.

4.1.2.3. Failure mode. Punching shear failure is generally known to be accompanied by a cone rupture surface, with a crack propagating from the bottom of the column-slab connection through to the top of the

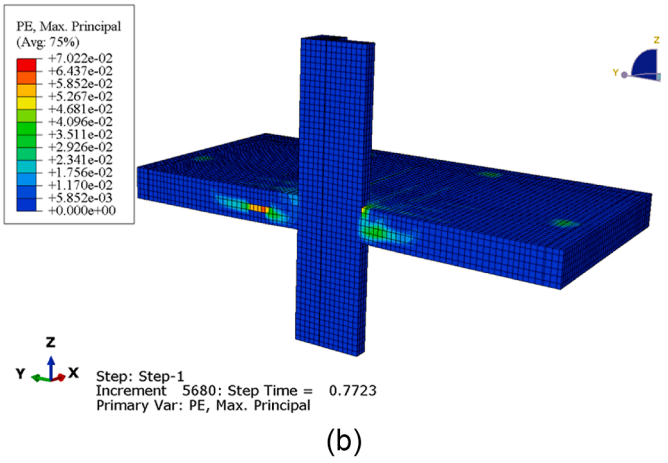


Fig. 11b. Crack pattern of T-shaped column specimen (Perspective).

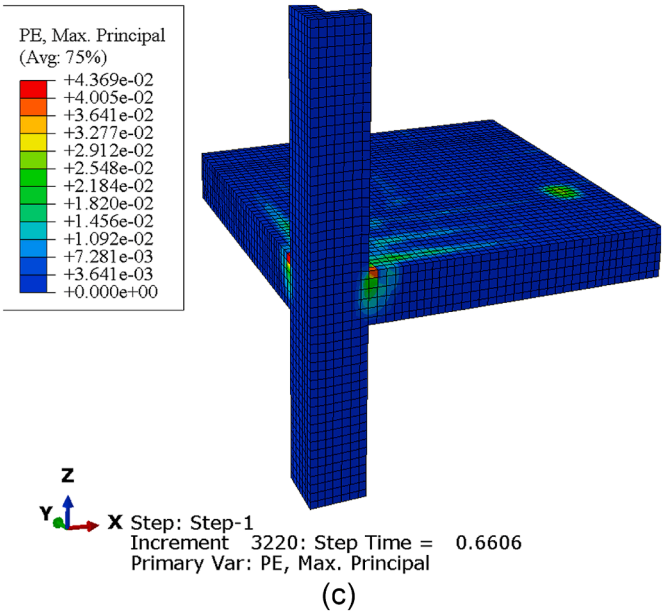


Fig. 11c. Crack pattern of Cruciform-shaped column specimen (Perspective).

cross-sectional slab inclined at 25°-30°. A physical inspection shows that the rupture surface in the finite element analysis was in good agreement with that obtained in the experimental test. Fig. 10 shows the rupture surface reported during the experimental research and the numerical results obtained in the course of this study.

4.2. Effects of different column shapes

4.2.1. Effect of column shapes on crack patterns and rupture

Similarly, to what was observed by Milligan et al. [51], It was generally observed in all models that permanent deformations are majorly concentrated on the peripherals of the columns with propagating cracks from the edges that form the shape of the column. The interior diagonal areas, to an extent, experienced no form of cracks (Fig. 11a-c). This implies that the column would punch through the slab and the inner section of the column perimeter would be moved along. The longest streak of cracks is formed in a similar shape to the column as it develops in a straight line reaching almost the edges of the slab. In Fig. 11c, it can be deduced that the cracking pattern was more pronounced along the rupture surface shown compared to what was observed in Fig. 10. Also, the punching cone formed was more extended

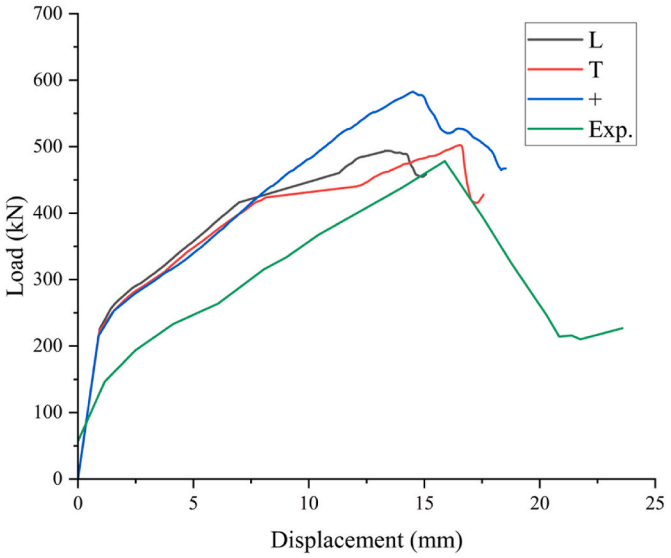


Fig. 12. Load-Displacement response of various flat slab specimen.

away from the column perimeter implying a larger cone area and higher values of the critical punching perimeter.

4.2.2. Effects of column shapes on reinforcement

As expected in the punching shear failure mechanism, the reinforcement stress distribution shows that although the reinforcements undergo a substantial magnitude of deformation they did not yield at the point of failure in all models. While the column reinforcements appear not to have been stressed at all even as it was part of the slab, most reinforcement deformations occur at positions near and through the column-slab connection. In the L-shape model, the stress in reinforcement at failure load was 501.7 N/mm^2. In the T-shape, the reinforcement stress was 501.8 N/mm^2 signifying just 0.1 N/mm^2 higher than in the L-shape specimen. The highest tensile stress in reinforcement was recorded in the Cruciform shape model with a value of 510 N/mm^2.

4.2.3. Effects on punching shear capacity

The punching shear capacities of various shapes were inferred from the peak load from which the slab fails in punching. It was noted that the failure loads of the various finite element models differ as 493.9 kN, 502.2 kN, and 582.8 kN was recorded for L, T, and Cruciform shape respectively. The results show there was generally a significant increase in the punching shear capacity of columns with the same loading area but different shapes. This observation is typical of the conclusion of Huang et al. [52] in their experimental research.

4.2.4. Effects on load-displacement response

In the load-displacement response as graphically represented in Fig. 12, it was revealed that all the finite element models exhibit similar responses in the earlier stages of loading. This shows a linear load-displacement relationship which is much stiffer compared to the experimental model. In the L-shape specimen, although, there was a significant drop in the load capacity of the slab the punching failure criterion was not accomplished by a very high sudden drop in load compared to other specimens. While the T-shape shows a much stiffer response in terms of load capacity in the punching stages of the slab, the cruciform shape shows a better stiffness in terms of displacement resistance. It can be deduced from the graph (Fig. 12) that the shape exhibits a closely related load-displacement response in reference to the experimental observations.

4.2.5. Code predictions and comparisons

The design codes considered in this study are ACI 318-19 [53], Euro

Table 6
Summary of Experimental, Finite element and Code predictions.

Slab	$V_{u(Exp.)}$ (kN)	$V_{u,FEA}$ (kN)	$\frac{V_{u,FEA}}{V_{u,FEA\ (Square)}}$	$V_{u,ACI\text{-}318\text{-}19M}$ (kN)	$V_{u,EC2,2004}$ (kN)	$Vu_{,MC2010(IV)}$ (kN)
Square	477.1	475.3	1.00	460.3	467.6	431.6
L-shape	–	493.9	1.03	497.5	484.3	438.4
T-Shape	–	502.2	1.05	482.6	487.4	394.3
Cross	–	582.8	1.23	444.2	473.2	389.5

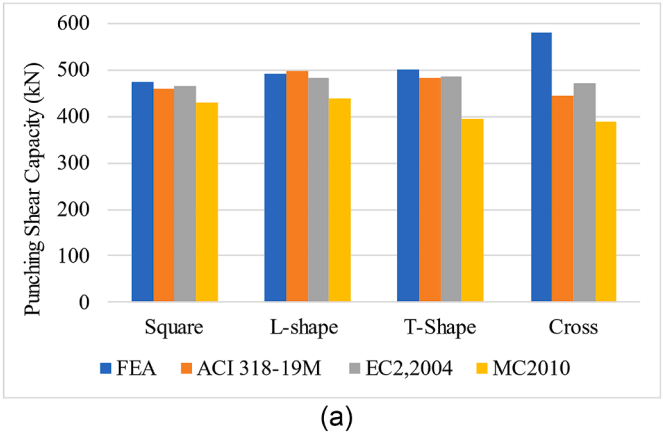


Fig. 13a. Comparison of punching shear capacity of different codes and with shapes.

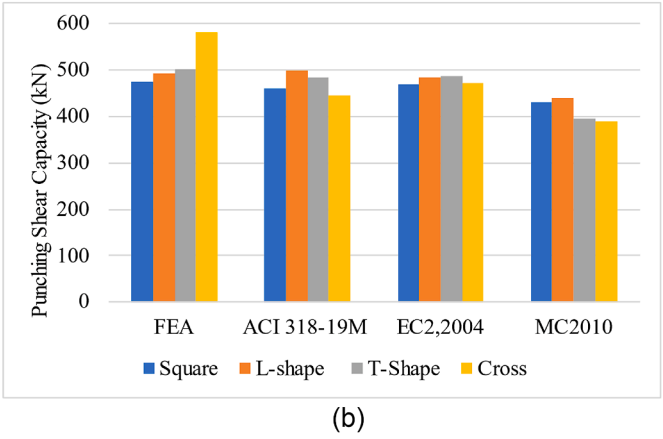


Fig. 13b. Comparison FEM, ACI 319-M, EC2 2004, MC 2010.

code 2–2004 [41] and Model code 2010 [54]. It is worth noting that the Level of Approximation IV adopted in the calculation of slab rotation while estimating the punching shear capacity from Model Code 2010. The code provisions for various shapes were applied and their respective predictions of punching shear capacity are presented in Table 6. In Fig. 13a, it was noted that relative to finite element results, the codes are slightly conservative to Square, L and T shapes. Meanwhile, in cruciform shape, there was high difference between the code predictions and FE results signifying that the effect of such a shape is underestimated. In the comparison presented in Fig. 13b, the finite element results predict flat slab supported by a cruciform-shaped column gives the highest punching resistance, as it descends across T-shape, L-shape and Square shape specimens respectively.

5. Conclusions

Numerical model of a flat slab was developed using Abaqus finite element software. The developed model was validated with existing experimental data from literature in terms of load-deflection response, failure mode, and crack patterns. The validated model was used to evaluate the parametric effects of column shapes, such as L, T, and Cruciform, on the punching shear response of flat slabs. The outcomes of the study were also compared with the existing code provisions. From the results of the study, the following conclusions are drawn:

1. The developed finite element model accurately simulate the punching shear behavior of reinforced concrete flat slabs with sufficient accuracy. The sensitivity analysis tests revealed that the best-suited dilation angle for the model is 25°, and the viscosity parameter is 0.0001.
3. The numerical results indicated that the support column geometry significantly influence the punching shear performance of flat slabs. The FE analysis results showed that L, T, and Cross shaped columns gave an increase of 3%, 5.3% and 22.6% respectively when compared to the square shaped column. Hence, compound column geometries can be effectively adopted to improve the punching shear resistance of flat slabs.
4. Apart from flat slabs supported on a cruciform shaped column, the punching shear values obtained from Eurocode 2, ACI 318-19 and MC 2010 model are in close proximity to the Finite Element results although MC 2010 gave the most conservative estimates. All the codes considered generally underestimates the punching shear capacity of the slab supported on Cruciform shaped column.
5. The observed failure pattern shows that cracks in flat slabs are usually of a radial form and the longest streak propagates from the corner edges of the column. Consequently, the shear stresses along the column perimeter were discovered to be focused at the corner edges of the supports.

Recommendation and further study

The primary focus of this research was to consider the effect of various column shapes on flat slabs with no shear reinforcements. Therefore, the effect of column geometry on flat slabs with shear reinforcements should be a subject of further study.

Declaration of competing interest

The authors declare no conflict of interest.

Data availability

Data will be made available on request.

Appendix A. Supplementary data

Supplementary data to this article can be found online at https://doi.org/10.1016/j.rineng.2023.101345.

References

[1] W.H. Mosley, J.H. Bungey, R. Hulse, Reinforced Concrete Design to Eurocode 2, ELBS with Macmillan, 2012.

[2] I al Daoor, Impact of COVID-19 on the contracting & engineering companies in gaza strip, Open J. Civ. Eng. 12 (2022) 75–86, https://doi.org/10.4236/OJCE.2022.121006.
[3] A.S. Genikomsou, M.A. Polak, Finite element analysis of punching shear of concrete slabs using damaged plasticity model in ABAQUS, Eng. Struct. 98 (2015) 38–48, https://doi.org/10.1016/j.engstruct.2015.04.016.
[4] S. Narayanan, Alternative punching shear reinforcement for RC flat slabs, Indian Concr. J. 88 (2014) 33–44.
[5] N.J. Gardner, Verification of punching shear provisions for reinforced concrete flat slabs, ACI Struct. J. 108 (2011) 572–580, https://doi.org/10.14359/51683214.
[6] T. Park, Inspection of collapse cause of Sampoong department store, Forensic Sci. Int. 217 (2011) 119–126, https://doi.org/10.1016/j.forsciint.2011.10.039.
[7] M.E. Criswell, C.E. Ospina, N.M. Hawkins, Behavior and Performance Levels of Reinforced Concrete Slab-Column Connections, American Concrete Institute, ACI Special Publication, 2016, pp. 35–58, https://doi.org/10.35789/fib.bull.0081.ch03, 2016- October, American Concrete Institute.
[8] M. Ramadan, D.M. Ors, A.M. Farghal, A. Afifi, A.H. Zaher, A.M. Ebid, Punching shear behavior of HSC & UHPC post tensioned flat slabs – an experimental study, Results Eng. 17 (2023), https://doi.org/10.1016/j.rineng.2023.100882.
[9] K.H. Yang, J.H. Mun, J.K. Song, S.H. Kim, S.H. Hwang, C.H. Chang, Punching shear capacity of lightweight aggregate concrete flat slabs without shear reinforcements 75 (2022) 296–309, https://doi.org/10.1680/JMACR.21.00324.
[10] A.K. Do, T.N. Nguyen, C.Q. Tran, H.T. Nguyen, D.X. Pham, Experimental and numerical investigations on the collapse behaviour of RC flat slab structures, Asian Journal of Civil Engineering 22 (2021) 1143–1155, https://doi.org/10.1007/S42107-021-00371-2.
[11] M.A. Polak, Ductility of Reinforced Concrete Flat Slab-Column Connections, vol. 20, 2005.
[12] M. Bastien-Masse, E. Brühwiler, Experimental investigation on punching resistance of R-UHPFRC–RC composite slabs, Materials and Structures/Materiaux et Constructions 49 (2016) 1573–1590, https://doi.org/10.1617/s11527-015-0596-4.
[13] P.M. Lewiński, P.P. Więch, Finite element model and test results for punching shear failure of RC slabs, Arch. Civ. Mech. Eng. 20 (2020), https://doi.org/10.1007/s43452-020-00037-x.
[14] Q. Zhang, G.J. Milligan, M.A. Polak, Nonlinear finite element analysis of punching shear strength of reinforced concrete slabs supported on L-shaped columns, Budownictwo i Architektura 19 (2020), https://doi.org/10.35784/bud-arch.2122.
[15] A.M. Sayed, Numerical study of the effects of flange damage on the steel beam capacity under static and fatigue flexural loads, Results Eng. 17 (2023), https://doi.org/10.1016/j.rineng.2022.100835.
[16] X. Cao, L. Wu, Z. Li, Behaviour of steel-reinforced concrete columns under combined torsion based on ABAQUS FEA, Eng. Struct. 209 (2020), 109980, https://doi.org/10.1016/j.engstruct.2019.109980.
[17] J.M. Graeme, M.A. Polak, C. Zurell, Impact of column rectangularity on punching shear strength: code predictions versus finite element analysis, J. Struct. Eng. 147 (2021), 04020331, https://doi.org/10.1061/(ASCE)ST.1943-541X, 0002889.
[18] M. Akinpelu, B. Ibitoye, O.O. Samson, K. Olorede, Numerical verification of strut and tie models and failure modes of reinforced self-compacting concrete deep beams, Int. J. Eng. Res. Afr. 53 (2021) 76–100.
[19] M. Alhassan, N. Betoush, N. Al-huthaifi, A. Al Dalou, Estimation of the fracture parameters of macro fiber-reinforced concrete based on nonlinear elastic fracture mechanics simulations, Results Eng. 15 (2022) 1–9, https://doi.org/10.1016/j.rineng.2022.100539.
[20] M.A. Akinpelu, A.A. Adedeji, Structural response of reinforced self - compacting concrete deep beam using finite element method, Journal of Soft Computing in Civil Engineering 2 (2018) 33–58.
[21] P.M. Beaulieu, G.J. Milligan, M.A. Polak, Using nonlinear finite element modeling for punching shear design of concrete slabs. Current perspectives and new directions in mechanics, modelling and design of structural systems - proceedings of the 8th international conference on structural engineering, Mechanics, and Computation (2022 2023) 1195–1200, https://doi.org/10.1201/9781003348443-194/USING-NONLINEAR-FINITE-ELEMENT-MODELING-PUNCHING-SHEAR-DESIGN-CONCRETE-SLABS-BEAULIEU-MILLIGAN-POLAK.
[22] A. Wosatko, J. Pamin, M. Anna, Application of damage – plasticity models in finite element analysis of punching shear, Comput. Struct. 151 (2015) 73–85, https://doi.org/10.1016/j.compstruc.2015.01.008.
[23] A.S. Genikomsou, M.A. Polak, Finite element analysis of punching shear of concrete slabs using damaged plasticity model in ABAQUS, Eng. Struct. 98 (2015) 38–48, https://doi.org/10.1016/j.engstruct.2015.04.016.
[24] R.K.S. Al Hamd, M. Gillie, H. Warren, G. Torelli, T. Stratford, Y. Wang, The effect of load-induced thermal strain on fl at slab behaviour at elevated temperatures, Fire Saf. J. 97 (2018) 12–18, https://doi.org/10.1016/j.firesaf.2018.02.004.
[25] R.K.S. Al-hamd, M. Gillie, L.S. Cunningham, H. Warren, A.S. Albostami, Novel shearhead reinforcement for slab-column connections subject to eccentric load and fire, Arch. Civ. Mech. Eng. 19 (2018) 503–524, https://doi.org/10.1016/j.acme.2018.12.011.
[26] HJN de Lima, Análise experimental da resistência a punção em lajes lisas com armadura de cisalhamento parcialmente ancorada, 2021.
[27] R. de A. Palhares, Análise experimental da punção em lajes lisas de concreto armado com variação da ancoragem da armadura de cisalhamento, 2018.
[28] R.A. Palhares, F.W. Rossignoli, G. Sales de Melo, H. Lima, A numerical model capable of accurately simulating the punching shear behavior of a reinforced concrete slab, Struct. Concr. 23 (2022) 1134–1150, https://doi.org/10.1002/SUCO.202100773.
[29] A. Genikomsou, Nonlinear Finite Element Analysis of Punching Shear of Reinforced Concrete Slab-Column Connections, 2016.
[30] D.W. Menna, A.S. Genikomsou, Punching shear response of concrete slabs strengthened with ultrahigh-performance fiber-reinforced concrete using finite-element methods, Pract. Period. Struct. Des. Construct. 26 (2021), https://doi.org/10.1061/(asce)sc.1943-5576.0000546.
[31] G. Milligan, Nonlinear Finite Element Analysis of Punching Shear of Reinforced Concrete Slabs Supported on Rectangular Columns, 2018.
[32] Dassault Systèmes, Concrete Damaged Plasticity - SIMULIA User Assistance 2021 n. D, 2021. https://help.3ds.com/2021/English/DSSIMULIA_Established/SIMACAEMATRefMap/simamat-c-concretedamaged.htm?contextscope=all. (Accessed 23 January 2023).
[33] B. Alfarah, F. López-Almansa, S. Oller, New methodology for calculating damage variables evolution in Plastic Damage Model for RC structures, Eng. Struct. 132 (2017) 70–86, https://doi.org/10.1016/J.ENGSTRUCT.2016.11.022.
[34] G.J. Milligan, M.A. Polak, C. Zurell, Finite element analysis of punching shear behavior of reinforced concrete slabs supported on walls, Struct. Concr. 23 (2022) 1118–1133, https://doi.org/10.1002/SUCO.202100692.
[35] M. Hafezolghorani, F. Hejazi, R. Vaghei, MS bin Jaafar, K. Karimzade, Simplified damage plasticity model for concrete, Struct. Eng. Int. 27 (2017) 68–78, https://doi.org/10.2749/101686616X1081.
[36] H. le Minh, S. Khatir, M. Abdel Wahab, T. Cuong-Le, A concrete damage plasticity model for predicting the effects of compressive high-strength concrete under static and dynamic loads, J. Build. Eng. 44 (2021), 103239, https://doi.org/10.1016/J.JOBE.2021.103239.
[37] A. Godat, O. Chaallal, Y. Obaidat, Non-linear finite-element investigation of the parameters affecting externally-bonded FRP flexural-strengthened RC beams, Results Eng. 8 (2020), https://doi.org/10.1016/j.rineng.2020.100168.
[38] M. Alhassan, N. Betoush, N. Al-Huthaifi, A. Al Dalou, Estimation of the fracture parameters of macro fiber-reinforced concrete based on nonlinear elastic fracture mechanics simulations, Results Eng. 15 (2022), https://doi.org/10.1016/j.rineng.2022.100539.
[39] J. Lubliner, J. Oliver, S. Oller, E. Oñate, A plastic-damage model for concrete, Int. J. Solid Struct. 25 (1989) 299–326, https://doi.org/10.1016/0020-7683(89)90050-4.
[40] J. Lee, G.L. Fenves, Plastic-damage model for cyclic loading of concrete structures, J. Eng. Mech. 124 (1998) 892–900, https://doi.org/10.1061/(ASCE)0733-9399(1998)124:8(892).
[41] B.S. Institution, EC for Standardization, Eurocode 2: Design of Concrete Structures : Part 1-1: General Rules and Rules for Buildings, British Standards Institution, 2004.
[42] H.A.W. Cornelissen, D.A. Hordijk, H.W. Reinhardt Summary, Experimental determination of crack softening characteristics of normalweight and lightweight concrete, Heron 31 (2) (1986) 1986.
[43] A. Genikomsou, M.A. Polak, Damaged Plasticity Modelling of Concrete in Finite Element Analysis of Reinforced Concrete Slabs, 2016, https://doi.org/10.21012/FC9.006.
[44] C. Ceb-Fip, Model Code 1990, Comite Euro-International Du Beton, 1991, pp. 87–109.
[45] A. Wosatko, A. Winnicki, M.A. Polak, J. Pamin, Role of dilatancy angle in plasticity-based models of concrete, Arch. Civ. Mech. Eng. 19 (2019) 1268–1283, https://doi.org/10.1016/J.ACME.2019.07.003.
[46] M.A. Akinpelu, A.A. Adedeji, Structural response of reinforced self-compacting concrete deep beam using finite element method, Journal of Soft Computing in Civil Engineering 2 (2018) 36–61, https://doi.org/10.22115/SCCE.2018.50115.
[47] M. Szczecina, A. Winnicki, Calibration of the CDP Model Parameters in Abaqus, 2015.
[48] A.S. Genikomsou, M.A. Polak, Finite element analysis of punching shear of concrete slabs using damaged plasticity model in ABAQUS, Eng. Struct. 98 (2015) 38–48, https://doi.org/10.1016/J.ENGSTRUCT.2015.04.016.
[49] P.M. Beaulieu, G.J. Milligan, M.A. Polak, Using nonlinear finite element modeling for punching shear design of concrete slabs. Current Perspectives and New Directions in Mechanics, Modelling and Design of Structural Systems, 1195–1200, https://doi.org/10.1201/9781003348443-194, 2022.
[50] Abaqus - SIMULIA User Assistance, 2021. https://help.3ds.com/2021/english/dssimulia_established/SIMULIA_Established_FrontmatterMap/sim-r-DSDocAbaqus.htm?contextscope=all&id=b15ba98a76ce4305b417ecdd54e5394d. (Accessed 14 February 2023).
[51] G.J. Milligan, M.A. Polak, C. Zurell, Finite element analysis of punching shear behavior of reinforced concrete slabs supported on walls, Struct. Concr. 23 (2022) 1118–1133, https://doi.org/10.1002/suco.202100692.
[52] C.-K. Huang, W.-T. Liu, Experimental Investigation on Behavior of Reinforced Concrete Slab-Column Connections with Columns of Cross-Shaped Section, vol. 45, Dalian Ligong Daxue Xuebao/Journal of Dalian University of Technology, 2005, pp. 580–586.
[53] 318-19 Building Code Requirements for Structural Concrete and Commentary, American Concrete Institute, 2019, https://doi.org/10.14359/51716937.
[54] International Federation for Structural Concrete (fib), Model Code 2010, final drafts, FIB Bulletin 1 & 2 (2013) 402.

View publication stats